An augmented iterative method for identifying a stress-free reference configuration in image-based biomechanical modeling

Manuel K. Rausch, Martin Genet, Jay D. Humphrey

An augmented iterative method for identifying a stress-free reference configuration in image-based biomechanical modeling

Manuel K. Rausch[a,*], Martin Genet[b], Jay D. Humphrey[a]

[a] *Department of Biomedical Engineering, Yale University*
[b] *Département de Méchanique, École Polytechnique Université Paris-Saclay*

Abstract

Continuing advances in computational power and methods have enabled image-based biomechanical modeling to become a crucial tool in basic science, diagnostic and therapeutic medicine, and medical device design. One of the many challenges of this approach, however, is the identification of a stress-free reference configuration based on in vivo images of loaded and often prestressed or residually stressed soft tissues and organs. Fortunately, iterative methods have been proposed to solve this inverse problem, among them Sellier's method. This method is particularly appealing for it is easy to implement, convergences reasonably fast, and can be coupled to nearly any finite element package. However, by means of several practical examples, we demonstrate that in its original formulation Sellier's method is not optimally fast and may not converge for problems with large deformations. Fortunately, we can also show that a simple, inexpensive augmentation of Sellier's method based on Aitken's delta-squared process can not only ensure convergence but also significantly accelerate the method.

Keywords: Inverse Methods, Fixed-Point Methods, Aitken's Delta-Squared Process, Stress-free Reference Configuration, Soft Tissue Mechanics

1. Introduction

Image-based biomechanical modeling has become a crucial tool in basic science, diagnostic and therapeutic medicine, and medical device design [1, 2, 3]. Ever improving image resolution and computational power increasingly enable models with greater detail. One key challenge remains, however. Tissues and organs, in vivo, are often prestressed and residually stressed in addition to experiencing time-varying in vivo loads [4, 5, 6]. Thus, the stress-free reference configuration is, in general, not readily accessible from in vivo images.

Fortunately, when the deformed configuration and its corresponding boundary conditions are known, the stress-free reference configuration can be estimated using inverse methods. These methods can be broadly classified either as direct methods, in which the inverse motion from the deformed configuration to the stress-free reference configuration is solved [7], or as iterative methods, which identify the stress-free reference configuration by employing multiple forward calculations (see [8, 9, 10] for a more comprehensive review). One such iterative method is a fixed-point method first introduced by Sellier [8] for general elasto-static problems and reintroduced by Bols et al [9] for problems in cardiovascular biomechanics. Sellier's method has since been applied successfully to a number of image-based biomechanical modeling problems, owing its success largely to algorithmic simplicity and the relative ease with which it can be coupled to established finite element software packages [11, 12].

In the first iteration Sellier applies the measured in vivo tractions (such as blood pressure, intraocular pressure, etc.) to a guessed initial reference configuration $\mathcal{B}_0^1$ with coordinates $\boldsymbol{X}^1$ to compute the first updated deformed configuration $\mathcal{B}_t^1$ with coordinates $\boldsymbol{x}^1$, see Figure 1. For lack of better alternatives, the initial reference configuration is usually chosen to be the measured in vivo configuration $\mathcal{B}_t^*$ with coordinates $\boldsymbol{x}^*$. Subsequently, the reference configuration is updated by subtracting the per node displacement vector between the updated deformed configuration and the target in vivo configuration, $\boldsymbol{R}^k = \boldsymbol{x}^k - \boldsymbol{x}^*$, viz. $\boldsymbol{X}^{k+1} = \boldsymbol{X}^k - \alpha \boldsymbol{R}^k$ (see Alogrithm 1, where Sellier chose $\alpha = 1$). This iterative procedure is then repeated until a required error tolerance ϵ is reached between the updated deformed configuration and the target in vivo configuration.

One of the advantages of Sellier's method is that any finite element package can be used to solve the forward problem, the only requirement being that the package can output nodal locations of the updated deformed configuration. A simple wrapper can then read the nodal locations, calculate the nodal displacement vector, update the reference configuration, and initiate the next forward calculation.

In their original manuscripts both Sellier and Bols as-

*Corresponding author
Email address: manuel.rausch@yale.edu (Manuel K. Rausch)

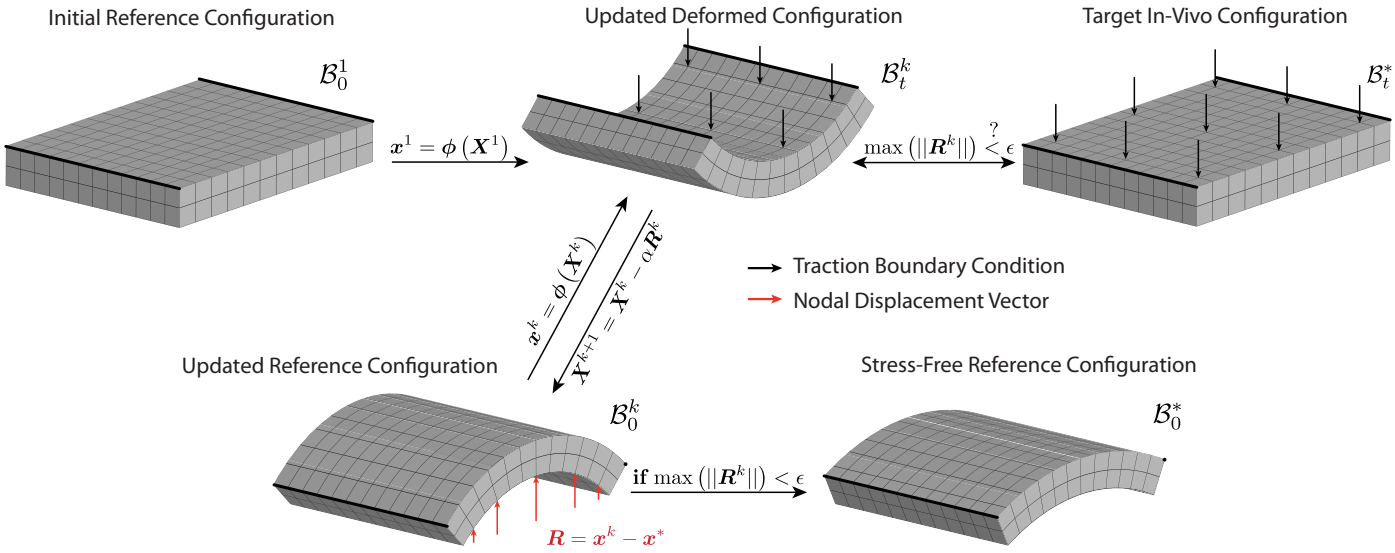

Figure 1: Illustration of Sellier's iterative method for identifying a stress-free reference configuration in biomechanical boundary value problems. See also Algorithm 1.

Algorithm 1 Sellier's Inverse Method (with $\alpha = 1$)

1: initialize $\boldsymbol{X}^1 \leftarrow \boldsymbol{x}^*$
2: set $k = 0$
3: **while** $\max(||\boldsymbol{R}^k||) \geq \epsilon$ **do**
4: update counter, $k \leftarrow k + 1$
5: solve forward problem, $\boldsymbol{x}^k = \boldsymbol{\phi}(\boldsymbol{X}^k)$
6: calculate nodal error vector, $\boldsymbol{R}^k = \boldsymbol{x}^k - \boldsymbol{x}^*$
7: update reference vector, $\boldsymbol{X}^{k+1} = \boldsymbol{X}^k - \alpha \boldsymbol{R}^k$
8: **end while**
9: stress-free reference configuration, $\boldsymbol{X}^* = \boldsymbol{X}^k$

sumed $\alpha = 1$ (see Algorithm 1). Here, we show that $\alpha = 1$ is not necessarily a good choice. Furthermore, we have previously combined Sellier's method with Aitken's delta-squared process and show here that by doing so Sellier's method can be considerably accelerate at virtually no cost [12].

2. Methods

In all subsequent examples we assume that the mechanical behavior of soft tissue can be well approximated using a hyperelastic framework. Furthermore, we specifically describe the material behavior using an anisotropic Fung-type strain energy function with an isotropic neo-Hookean component and n embedded fiber families [13, 14, 15]. The isochoric component of the strain energy function, $\mathcal{W}(\boldsymbol{C}) = \bar{\mathcal{W}}(\bar{\boldsymbol{C}}) + U(J)$, thus reads [16]

$$\bar{\mathcal{W}} = \frac{\mu}{2}[\bar{I}_1 - 3] + \sum_{i=1}^{n} \frac{k_1^i}{4k_2^i}\left[\exp\left(k_2^i\left[\bar{I}_4^i - 1\right]^2\right) - 1\right], \quad (1)$$

where $\bar{I}_1$ is the first invariant of the isochoric right Cauchy-Green tensor, $\bar{I}_1 = \bar{\boldsymbol{C}} : \boldsymbol{I}$, and $\bar{I}_4^i$ are the squares of the fiber stretches of each fiber family, $\bar{I}_4^i = \bar{\boldsymbol{C}} : \boldsymbol{M}^i \otimes \boldsymbol{M}^i$, with $\boldsymbol{M}^i$ the unit fiber orientation vectors. In addition, we constrain all materials to behave quasi-incompressibly by penalizing the volumetric material response with a bulk modulus $\kappa >> \mu$ in the volumetric term $U(J) = \frac{1}{2}\kappa\left[\ln J\right]^2$, where $J = \det \boldsymbol{F}$.

Also, we solve all forward problems employing the open-source finite element packages FEBio (www.febio.org) and use Matlab for all auxiliary tasks [17].

We begin our analysis with a canonical problem inspired by our recent histomechanical study of occlusive venous thrombi in mice. Given the in vivo measured length of a nearly cylindrical thrombus sample and venous blood pressure p (length: 4mm, diameter: 1.2mm, load: 10-30mmHg), we aim to determine the thrombus' stress-free reference configuration. To simplify the problem, we reduce the geometry to a quarter cylinder with traction free radial surface and tractions due to venous blood pressure on the proximal and distal surfaces. We further discretize this simplified geometry with 384 trilinear hexahedral elements and employ the hyperelastic framework to model the thrombus as a quasi-incompressible, neo-Hookean material with a shear modulus based on recent measurements in our laboratory [18] (see Equation (1) with $k_1^i = 0$ for the strain energy function of a quasi-incompressible neo-Hookean material).

To explore the influence of ϵ, α, and the magnitude of deformation on the convergence of Sellier's method, we apply Algorithm 1 to above problem for varying α, $\epsilon = 0.01, 0.001, 0.0001$, and $p = 10, 20, 30$mmHg.

Next, we augment Sellier's method by dynamically adapting α according to Aitken's delta-squared process, which has previously been proven an efficient acceleration method for fluid-structure interaction problems and prob-

lems in nonlinear solid mechanics [19, 20]. Thus, in Algorithm 1, we add a step after calculating the nodal displacement vector, in which we update α according to

$$\alpha \leftarrow -\alpha \frac{\boldsymbol{R}^{k-1} \cdot \left[\boldsymbol{R}^{k} - \boldsymbol{R}^{k-1}\right]}{\left[\boldsymbol{R}^{k} - \boldsymbol{R}^{k-1}\right] \cdot \left[\boldsymbol{R}^{k} - \boldsymbol{R}^{k-1}\right]}, \qquad (2)$$

see Algorithm 2. For the augmented method, we repeat the same sensitivity analysis as above.

In our second example, we explore Sellier's method as well as our augmented method by virtue of a practical, yet, simple example from our laboratory. Specifically, we apply Sellier's method to the quasi-static boundary value problem of a pressurized, axially prestretched healthy mouse arterial segment that we recently tested in our laboratory. Albeit, technically not an inverse problem since the stress-free reference configuration is known, we imagine, for argument sake, that in addition to the material parameters only the in vivo target configuration as well as the luminal pressure and the axial prestretch are known. We model the arterial segment as a perfect quarter cylinder (length: 3.80mm, inner diameter: 0.57mm, wall thickness: 45.2μm, load: 80mmHg, axial prestretch: 1.77), discretized with 3072 trilinear hexahedral elements, and assume that the material is well approximated using the hyperelastic framework (see Equation (1) with $n = 4$). Here, we limit our analysis to the effect of α only ($\epsilon = 0.01$mm).

In our third example, we apply Sellier's method as well as the augmented method to a problem in heart valve mechanics taken from Rausch et al [21]. In this example, the anterior ovine mitral valve, reconstructed from in vivo marker data, is exposed to systolic left ventricular pressure (100mmHg, also measured in vivo) and isotropic prestrain (30%) [22, 23]. The leaflet is modeled as a transversely isotropic, thin, collagenous membrane and discretized with 1920 quadratic triangular elements. The material behavior is, again, approximated using the strain energy function in Equation (1). Note, only one fiber family is modeled in this example ($n = 1$). In addition to traction boundary condition on the ventricularis (the ventricular side of the leaflet), Dirichlet boundary conditions are applied to the external boundary of the leaflet as derived from the marker data. Neo-Hookean, 1D elements approximate the behavior of the chordae tendinae that emanate from the papillary muscles and insert in the belly regions of the leaflet. For more details see [22].

Last, we apply Sellier's method and the augmented method to an actual inverse problem from our laboratory. We derive the geometry of a murine aortic dissection from a combined in vivo (ultrasound) and ex vivo (optical coherence tomography) imaging approach. Note, at the time of imaging the dissected aorta segmented was axially prestretched and subjected to intraluminal pressure (length: 7.82mm, load: 80mmHg, axial prestretch: 1.50). For the present analysis we, again, assume that we can describe the aortic material behavior using the strain energy function in Equation (1) with $n = 4$. In contrast to the dissected aortic wall, we model the intramural thrombus as neo-Hookean. We assume the thrombus, like the aortic wall, is quasi-incompressible. Further, we spatially discretize the dissected aortic wall segment and thrombus complex with 141,661 10-node, quadratic, tetrahedral elements [24] and solve the forward problem using FEBio, as above. As opposed to the previous problem, however, we do not perform a sensitivity analysis. Instead, based on the findings in Figure 2, we chose $\alpha = 0.5$ and $\alpha = 1.0$ for both, Sellier's method and the augmented method ($\epsilon = 0.1$mm).

Algorithm 2 Augmented Sellier's Inverse Method

initialize $\boldsymbol{X}^1 \leftarrow \boldsymbol{x}^*$
set $k = 0$
while $\max\left(||\boldsymbol{R}^k||\right) \geq \epsilon$ **do**
  update counter, $k \leftarrow k + 1$
  solve forward problem, $\boldsymbol{x}^k = \boldsymbol{\phi}(\boldsymbol{X}^k)$
  calculate nodal error vector, $\boldsymbol{R}^k = \boldsymbol{x}^k - \boldsymbol{x}^*$
  if $k > 1$ **then**
    update alpha, $\alpha \leftarrow -\alpha \frac{\boldsymbol{R}^{k-1} \cdot \left[\boldsymbol{R}^{k} - \boldsymbol{R}^{k-1}\right]}{\left[\boldsymbol{R}^{k} - \boldsymbol{R}^{k-1}\right] \cdot \left[\boldsymbol{R}^{k} - \boldsymbol{R}^{k-1}\right]}$
  end if
  update reference vector, $\boldsymbol{X}^{k+1} = \boldsymbol{X}^k - \alpha \boldsymbol{R}^k$
end while
stress-free reference configuration, $\boldsymbol{X}^* = \boldsymbol{X}^k$

3. Results

Figure 2A illustrates the convergence behavior of both Sellier's method and our augmented method as a function of α ($\epsilon = 0.01$mm and $p = 30$mmHg). First, we find that in Sellier's original formulation, the number of iterations necessary to reach convergence varies significantly with α, with a minimum at $\alpha = 1.1$. Second, we find that the augmented method convergences almost independently of the initial value of α and converges faster than Sellier's method for all values of α except for $\alpha = 1.1$, where both method converge equally fast. Last, we find that the convergence radius for Sellier's method is $\rho_\alpha \leq 1.7$, whereas the convergence radius for the augmented method is $\rho_\alpha > 1.7$ (data not shown).

Maybe not surprisingly, we also find that the number of iterations increases as we tighten the convergence criterion. Similarly, the number of iterations increases with increasing load and thus deformation. Interestingly, for both methods, the optimal α as well as the convergence radius ρ_α are invariant to ϵ and p, at least for the tested values. Also, the augmented method always convergences faster than Sellier's method except for the optimal α, where Sellier's method and the augmented method convergence almost equally fast (with the augmented method having a slight edge for $\epsilon = 0.001$mm and $\epsilon = 0.0001$mm).

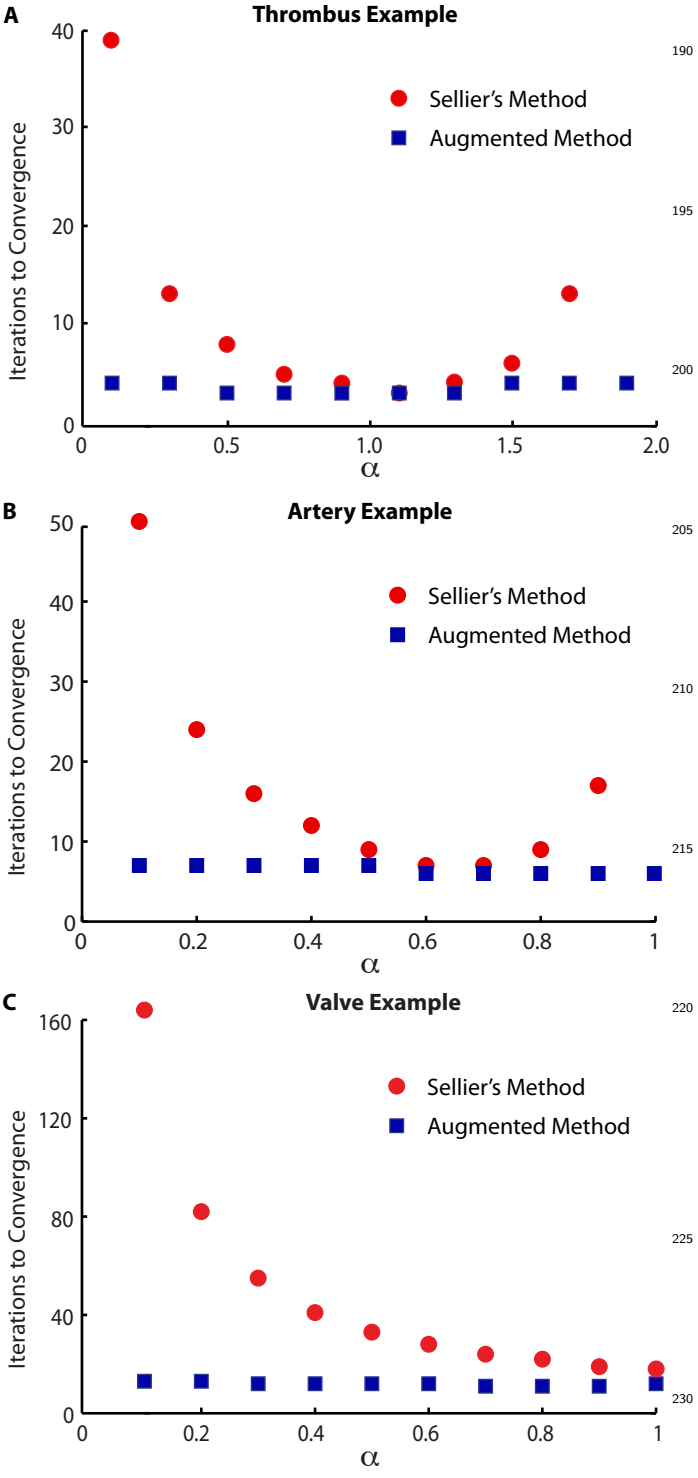

Figure 2: For Sellier's method the number of iterations to convergence strongly depends on α and is always larger or equal the number of iterations necessary for our augmented method. Furthermore, the augmented method is virtually independent of α and shows a larger convergence radius.

The findings from our second example are summarized in Figure 2B. Confirming the results of the previous example, we find that in Sellier's original formulation the number of iterations necessary to reach convergence varied significantly with α, with the smallest number of iterations at $\alpha = 0.6, 0.7$. Also, for $\alpha = 1$ the method failed to converge, again, demonstrating a limited convergence radius. In accordance with the previous example, we further find that our augmented method is virtually insensitive to the choice of α and converges always faster than Sellier's original formulation, albeit, not significantly for $\alpha = 0.6, 0.7$. Additionally, our method converged for $\alpha = 1$, demonstrating, again, a larger convergence radius.

Our third example confirms most findings of the previous two examples, see Figure 2C. Our augmented method results in faster convergence than Sellier's method, whose convergence strongly depends on α. While Sellier's method converges only for values of $\alpha \leq 1$, our augmented method convergences for values $\alpha > 1$. Noteworthily, the qualitative behavior of the α-dependence of Sellier's method is different from the previous two examples in that the number of iterations appear to converge asymptotically toward the minimum.

Last, applied to the real-world inverse analysis problem of the prestretched and pressurized aortic dissection (Figure 3A), for $\alpha = 0.5$ Sellier's method converges in five iterations, while our augmented method converges in four iterations; for $\alpha = 1.0$ Sellier's method fails to converge, while our augmented method converges in five iterations. Thus, here again, our method converges faster than Sellier's method and shows a larger convergence radius. Figure 3B shows the updated deformed configurations ($k = 1..4$) for our augmented method with $\alpha = 0.5$ and demonstrates convergence of the updated deformed configuration toward the target in vivo configuration.

4. Discussion

Sellier's method is a simple, yet efficient method for the inverse identification of a stress-free reference configuration as usually required for image-based biomechanical analyses. However, both Sellier, in the original work, as well as Bols et al, who reintroduced Sellier's method specifically for biomechanical problems, assumed $\alpha = 1$.

In four practical examples we demonstrate that Sellier's method with $\alpha = 1$ may result in suboptimal convergence rates and in some examples may fail to converge altogether. Thus, $\alpha = 1$ may not be the optimal choice for Sellier's method. We also find that the optimal α is problem dependent without means of a priori determination. Our augmented method may mitigate these shortcomings. We were able to demonstrate that dynamically adapting α via Aitken's delta-squared process increases the convergence rate of Sellier's method almost independently of α as well as increases the convergence radius [25].

Augmenting Sellier's method may guarantee convergence and significantly accelerates convergence and thus provides significant time savings for large problems. Hence, given that our augmentation comes at virtually

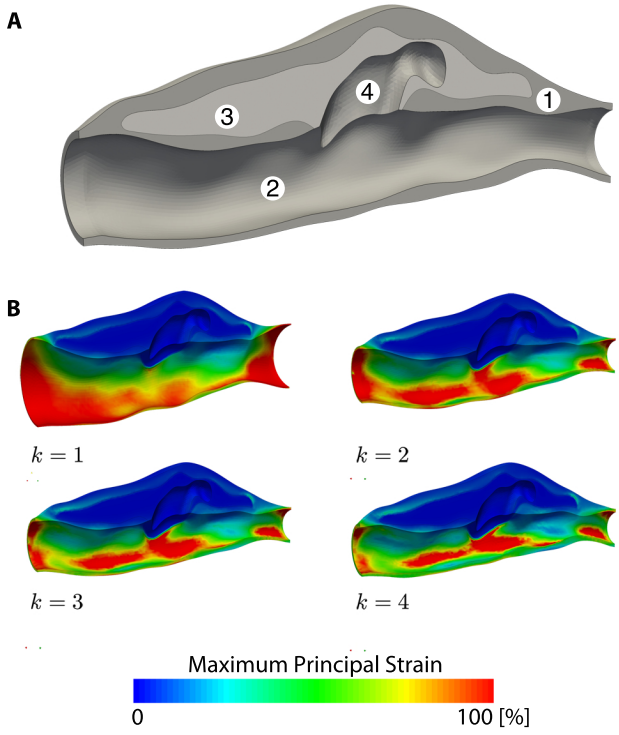

Figure 3: A) Loaded in vivo geometry of a murine aortic dissection derived from in vivo ultrasound and ex vivo optical coherence tomography with (1) aortic wall, (2) aortic lumen, (3) intramural thrombus, and (4) false lumen. B) Convergence of the updated deformed configuration ($k = 1..4$) for our augmented method ($\alpha = 0.5$), where convergence occurred at iteration $k = 4$.

no cost and requires almost no additional effort for implementation, biomechanicians considering Sellier's method should apply the augmentation proposed in this work.

Acknowledgment

This work was funded, in part, by NIH grants R01 HL086418, U01 HL116323, and T32 HL007974. We also thank Dr. Matthew R. Bersi and Dr. Paolo Di Achille for providing data for some of the examples in this manuscript.

References

[1] B. Baillargeon, I. Costa, J. R. Leach, L. C. Lee, M. Genet, A. Toutain, J. F. Wenk, M. K. Rausch, N. Rebelo, G. Acevedo-Bolton, et al., Human cardiac function simulator for the optimal design of a novel annuloplasty ring with a sub-valvular element for correction of ischemic mitral regurgitation, Cardiovascular Engineering and Technology 6 (2) (2015) 105–116.

[2] M. K. Rausch, A. M. Zöllner, M. Genet, B. Baillargeon, W. Bothe, E. Kuhl, A virtual sizing tool for mitral valve annuloplasty, International Journal for Numerical Methods in Biomedical Engineering.

[3] B. Bosmans, N. Famaey, E. Verhoelst, J. Bosmans, J. Vander Sloten, A validated methodology for patient specific computational modeling of self-expandable transcatheter aortic valve implantation, Journal of Biomechanics 49 (13) (2016) 2824–2830.

[4] H. Han, Y. Fung, Residual strains in porcine and canine trachea, Journal of Biomechanics 24 (5) (1991) 307–315.

[5] C. Bellini, J. Ferruzzi, S. Roccabianca, E. Di Martino, J. Humphrey, A microstructurally motivated model of arterial wall mechanics with mechanobiological implications, Annals of Biomedical Engineering 42 (3) (2014) 488–502.

[6] A. B. Tepole, M. Gart, C. A. Purnell, A. K. Gosain, E. Kuhl, The incompatibility of living systems: Characterizing growth-induced incompatibilities in expanded skin, Annals of Biomedical Engineering 44 (5) (2016) 1734–1752.

[7] S. Govindjee, P. A. Mihalic, Computational methods for inverse finite elastostatics, Computer Methods in Applied Mechanics and Engineering 136 (1) (1996) 47–57.

[8] M. Sellier, An iterative method for the inverse elasto-static problem, Journal of Fluids and Structures 27 (8) (2011) 1461–1470.

[9] J. Bols, J. Degroote, B. Trachet, B. Verhegghe, P. Segers, J. Vierendeels, A computational method to assess the in vivo stresses and unloaded configuration of patient-specific blood vessels, Journal of Computational and Applied Mathematics 246 (2013) 10–17.

[10] S. A. Maas, A. Erdemir, J. P. Halloran, J. A. Weiss, A general framework for application of prestrain to computational models of biological materials, Journal of the Mechanical Behavior of Biomedical Materials 61 (2016) 499–510.

[11] A. Wittek, K. Karatolios, P. Bihari, T. Schmitz-Rixen, R. Moosdorf, S. Vogt, C. Blase, In vivo determination of elastic properties of the human aorta based on 4d ultrasound data, Journal of the mechanical behavior of biomedical materials 27 (2013) 167–183.

[12] M. Genet, M. Rausch, L. Lee, S. Choy, X. Zhao, G. Kassab, S. Kozerke, J. Guccione, E. Kuhl, Heterogeneous growth-induced prestrain in the heart, Journal of Biomechanics 48 (10) (2015) 2080–2089.

[13] G. A. Holzapfel, T. C. Gasser, R. W. Ogden, A new constitutive framework for arterial wall mechanics and a comparative study of material models, Journal of Elasticity and the Physical Science of Solids 61 (1-3) (2000) 1–48.

[14] M. Rausch, G. Karniadakis, J. Humphrey, Modeling soft tissue damage and failure using a combined particle/continuum approach, Biomechanics and Modeling in Mechanobiology (2016) 1–13.

[15] A. W. Caulk, J. B. Dixon, R. L. Gleason Jr, A lumped parameter model of mechanically mediated acute and long-term adaptations of contractility and geometry in lymphatics for characterization of lymphedema, Biomechanics and Modeling in Mechanobiology (2016) 1–18.

[16] M. K. Rausch, E. Kuhl, On the mechanics of growing thin biological membranes, Journal of the Mechanics and Physics of Solids 63 (2014) 128–140.

[17] S. A. Maas, B. J. Ellis, G. A. Ateshian, J. A. Weiss, Febio: finite elements for biomechanics, Journal of Biomechanical Engineering 134 (1) (2012) 011005.

[18] Y.-U. Lee, A. Lee, J. Humphrey, M. Rausch, Histological and biomechanical changes in a mouse model of venous thrombus remodeling, Biorheology 52 (3) (2015) 235–245.

[19] U. Küttler, W. A. Wall, Fixed-point fluid-structure interaction solvers with dynamic relaxation, Computational Mechanics 43 (1) (2008) 61–72.

[20] M. Genet, L. Marcin, P. Ladeveze, On structural computations until fracture based on an anisotropic and unilateral damage theory, International Journal of Damage Mechanics 23 (4) (2014) 483–506.

[21] M. K. Rausch, W. Bothe, J.-P. E. Kvitting, S. Göktepe, D. C. Miller, E. Kuhl, In vivo dynamic strains of the ovine anterior mitral valve leaflet, Journal of Biomechanics 44 (6) (2011) 1149–1157.

[22] M. K. Rausch, N. Famaey, T. O. Shultz, W. Bothe, D. C. Miller, E. Kuhl, Mechanics of the mitral valve, Biomechanics and Modeling in Mechanobiology 12 (5) (2013) 1053–1071.

[23] R. Amini, C. E. Eckert, K. Koomalsingh, J. McGarvey, M. Mi-

nakawa, J. H. Gorman, R. C. Gorman, M. S. Sacks, On the in vivo deformation of the mitral valve anterior leaflet: effects of annular geometry and referential configuration, Annals of Biomedical Engineering 40 (7) (2012) 1455–1467.

[24] S. A. Maas, B. J. Ellis, D. S. Rawlins, J. A. Weiss, Finite element simulation of articular contact mechanics with quadratic tetrahedral elements, Journal of Biomechanics 49 (5) (2016) 659–667.

[25] A. C. Aitken, On the iterative solution of a system of linear equations, Proceedings of the Royal Society of Edinburgh. Section A. Mathematical and Physical Sciences 63 (01) (1950) 52–60.